Proceedings of the 7th International Conference on Asian and Pacific Coasts
(APAC 2013) Bali, Indonesia, September 24-26, 2013

NUMERICAL ANALYSIS OF TSUNAMI-INDUCED INUNDATION BEHIND BUILDINGS ALONG COASTS

T. Nakamura[1], N. Mizutani[2], N. Hirakawa[3] and S. Ashizawa[4]

ABSTRACT: To evaluate the effects of impermeable rigid buildings located near vertical quay walls on the reduction of the inundation water volumes due to run-up tsunamis, a full-scale three-dimensional numerical analysis is performed using a three-dimensional coupled fluid-structure-sediment interaction model. Numerical results show that the inundation water volume can be reduced with an increase in the shielding ratio of the long-shore width of the buildings with respect to the total width of the coastline, and accordingly the buildings located along the coasts have the reduction effects of the inundation water volume. This suggests that countermeasures against tsunamis can be evaluated in a comprehensive manner in terms of not only shore protection facilities for tsunamis at relatively high frequencies but also such buildings. Furthermore, the inundation depth at the seaward side of the buildings and the cross-shore bottom flow velocity at the gaps between the buildings increase with the shielding ratio, suggesting an increase in tsunami force and the onset of local scouring when the shielding ratio is large. Consequently, when designing buildings along the coasts, it is essential to consider an appropriate balance between the reduction effects of the inundation water volume and the instability of the buildings caused by the tsunami force and the local scouring.

Keywords: Tsunami, inundation, building, disaster mitigation, three-dimensional numerical analysis.

INTRODUCTION

A series of massive tsunamis triggered by the 2011 Tohoku earthquake resulted in a catastrophic disaster along the northwest coast of the Honshu Island, Japan. To deal with such massive tsunamis, the concept of disaster mitigation using multifaceted countermeasures to reduce the run-up of tsunamis to the best possible extent is more important than the construction of shore protection facilities for tsunamis at relatively high frequencies. This paper focuses on one of such concepts, which involves rigid buildings located along the coasts. Such buildings are expected to be effective to mitigate damage from the run-up of tsunamis because of the complementation of shore protection facilities by reducing inundation areas and depths of the tsunamis. However, no quantitative evaluation of the tsunami reduction effects of such buildings is available.

In this study, a full-scale three-dimensional (3-D) numerical analysis is performed using a 3-D coupled fluid-structure-sediment interaction model (Nakamura et al. 2011) to quantitatively evaluate the effects of rigid buildings located near quay walls on the reduction of the inundation water volumes due to run-up tsunamis.

NUMERICAL MODEL

The 3-D coupled fluid-structure-sediment interaction model (Nakamura et al. 2011) is composed of a main solver and three modules. The main solver is a large-eddy simulation (LES) model based on extended continuity and momentum equations for incompressible viscous air-water two-phase flow that considers seepage flow in porous media, the motion of a movable structure, and the profile evolution of the seabed. The first module is a volume-of-fluid (VOF) module based on the multi-interface advection and reconstruction solver (MARS; Kunugi 2000) for air-water interface tracking. The second module is an immersed-boundary (IB) module based on the volume-force type of IB method (Kajishima and Takiguchi 2002) for the motion of the movable structure. The third module is a sediment transport module for computing the profile evolution of the seabed induced by bed-load and suspended sediment transport and the motion of suspended sediment transport that considers all transport processes of pick-up, advection, diffusion, and settling. In the model, the three modules are connected to the main solver using a two-way coupling procedure implemented at every time step to ensure fluid-structure-sediment interaction. In this study, the main solver and the VOF module were used not to simulate movable structures and sediment transport. For

[1] Institute for Advanced Research, Nagoya University, Furo-cho, Chikusa-ku, Nagoya 464-8601, JAPAN
[2] Department of Civil Engineering, Nagoya University, Furo-cho, Chikusa-ku, Nagoya 464-8603, JAPAN
[3] Executive Officer, Maeda Corporation, J. CITY 5-8, Takamatsu, Nerima-ku, Tokyo 179-8903, JAPAN
[4] Maeda Corporation, J. CITY 5-8, Takamatsu, Nerima-ku, Tokyo 179-8903, JAPAN

completeness, an overview of the main solver and the VOF module is presented below. Detailed explanation of the model can be found in Nakamura et al. (2011).

The volume porosity m representing the volume fraction of void space in each cell ($0 \le m \le 1$, where m = 0 for pure impermeable solids, $0 < m < 1$ for porous media, and m = 1 for pure fluids) is assumed to be equal to the surface porosity. In addition, temporal variation in the porosity is assumed to be sufficiently small ($\partial m/\partial t$ = 0). Based on these assumptions, the extended governing equations for continuity, momentum, and air-water interface motion are given as follows:

$$\frac{\partial(mv_j)}{\partial x_j} = q^* \tag{1}$$

$$\{m + C_A(1-m)\}\frac{\partial v_i}{\partial t} + \frac{\partial(mv_iv_j)}{\partial x_j} = -\frac{m}{\hat{\rho}}\frac{\partial p}{\partial x_i} + mg_i + \frac{m}{\hat{\rho}}\left(f_i^s + R_i + f_i^{ob}\right) + \frac{1}{\hat{\rho}}\frac{\partial}{\partial x_j}\left(2m\hat{\mu}D_{ij}\right) + \frac{\partial}{\partial x_j}\left(-m\tau_{ij}^a\right) + Q_i + m\beta_i \tag{2}$$

$$m\frac{\partial F}{\partial t} + \frac{\partial(mv_jF)}{\partial x_j} = Fq^* \tag{3}$$

in which v_i is the fluid/seepage flow velocity vector, p is the pressure, x_i is the position vector (= $[x\ y\ z]^T$), t is the time, g_i is the gravitational acceleration vector (= $[0\ 0\ -g]^T$, g is the gravitational acceleration), $\hat{\rho}$ is the density of fluid (= $F\,\rho_w + (1-F)\,\rho_a$, ρ_w and ρ_a are the densities of water and air), $\hat{\mu}$ is the molecular viscosity of fluid (= $F\,\mu_w + (1-F)\,\mu_a$, μ_w and μ_a are the molecular viscosities of water and air), C_A is the added mass coefficient (Mizutani et al. 1996), R_i is the laminar and turbulent resistance force vector due to porous media (Mizutani et al. 1996), f_i^s is the surface tension force vector based on the continuum surface force (CSF) model (Brackbill et al. 1992), D_{ij} is the strain rate tensor (= $\partial v_i / \partial x_j + \partial v_j / \partial x_i$), τ_{ij} is the turbulent stress tensor based on the dynamic two-parameter mixed model (DTM; Horiuti 1997), q^* is the intensity of wave generation source/sink per unit of time (Kawasaki 1999), Q_i is the wave generation source/sink vector, β_i is the artificial damping factor vector (= $[0\ 0\ -\beta w]^T$, β is the artificial damping factor), and superscript a is the anisotropic part of a tensor. In deriving these equations, the spatial variation in the porosity is taken into account ($\partial m/\partial x_i \ne 0$) to capture possible sharp changes in the porosity around the surface of the porous media. However, based on the formulation of CADMAS-SURF (CDIT 2001), the spatial variation in the porosity is assumed to be negligible ($\partial m/\partial x_i$ = 0) only in deriving the pressure gradient term of the momentum conservation equation (the first term on the right-hand side of Eq. (2)). This is to ensure equilibrium between the pressure gradient term and the gravitational acceleration term (the second term on the right-hand side of Eq. (2)) in still water regardless of the spatial changes in the porosity. In Eq. (2), f_i^s, R_i, and Q_i are given as

$$f_i^s = \sigma\kappa\frac{\partial F}{\partial x_i}\frac{\hat{\rho}}{\rho_{avg}} \tag{4}$$

$$R_i = -\frac{12C_{D2}\hat{\mu}(1-m)}{md_{50}^2}v_i - \frac{C_{D1}\hat{\rho}(1-m)}{2md_{50}}v_i\sqrt{v_jv_j} \tag{5}$$

$$Q_i = v_iq^* - \frac{2}{3}\frac{\partial}{\partial x_i}\left(m\hat{\nu}\frac{\partial v_j}{\partial x_j}\right) \tag{6}$$

in which σ is the surface tension coefficient, κ is the local surface curvature, ρ_{avg} is the density of fluid at the air-water interface (= $(\rho_w + \rho_a) / 2$), C_{D2} and C_{D1} are the laminar and turbulent resistance coefficients (Mizutani et al. 1996), d_{50} is the median grain size of sediment particles, and $\hat{\nu}$ is the molecular kinematic viscosity of fluid (= $\hat{\rho}/\hat{\mu} = F\,\nu_w + (1-F)\,\nu_a$, ν_w and ν_a are the molecular kinematic viscosities of water and air). Defining the grid-scale filter as the overbar, τ^a_{ij} in Eq. (2) is given as

$$\tau_{ij}^a = L_{ij}^{ma} + C_BL_{ij}^{Ra} - C_S|D|D_{ij} \tag{7}$$

$$L_{ij}^m = \overline{\bar{v}_i\bar{v}_j} - \bar{\bar{v}}_i\,\bar{\bar{v}}_j \tag{8}$$

$$L_{ij}^R = \overline{\left(v_i - \bar{v}_i\right)\left(v_j - \bar{v}_j\right)} - \overline{\left(v_i - \bar{v}_i\right)}\,\overline{\left(v_j - \bar{v}_j\right)} \tag{9}$$

in which $|D|$ is the absolute value of the strain rate tensor D_{ij}, and C_B and C_S are the non-dimensional coefficients, which are dynamically computed from the value of v_i at each time step (Horiuti, 1997).

COMPUTATIONAL DOMAIN AND CONDITIONS

This study focused on a simple geography shown in Fig. 1. Specifically, an impermeable vertical quay wall that had a freeboard h_f of 3.0 m when the water level was at the low water level (LWL) of h_l was set 1 km onshore from a wave generation source/sink, and an impermeable horizontal flat land with a cross-shore length of 150.0 m was set behind it. Subsequently, buildings with a cross-shore length of l_b were fixed at a distance of x_b from the quay wall on the land. For simplicity, the buildings were sufficiently-high impermeable rigid rectangular objects with no openings such as windows. To avoid the reflection from the offshore boundary, an artificial damping zone with a cross-shore length of 1 km was set at the offshore side of the wave generation source/sink. To measure the inundation water volumes, a wave

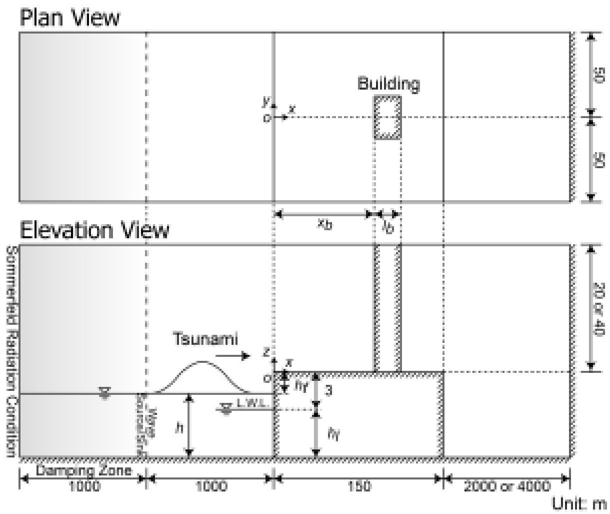

Fig. 1 Computational domain

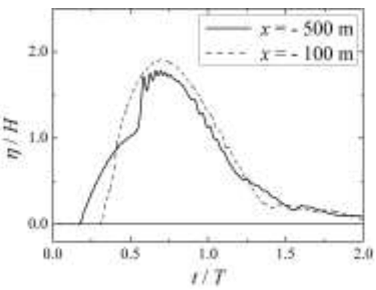

Fig. 2 Water surface fluctuation η at y = 0 m in front of the quay wall for H = 5.0 m, T = 300.0 s, h_l = 7.5 m, and h_f = 1.5 m with no buildings

Table 1 Computational conditions

H [m]	T [s]	h_l [m]	h_f [m]	x_b [m]	l_b [m]
3.0	60.0	7.5	1.5	100.0	20.0
3.0	180.0	7.5	1.5	100.0	20.0
3.0	300.0	7.5	1.5	100.0	20.0
3.0	420.0	7.5	1.5	100.0	20.0
3.0	540.0	7.5	1.5	100.0	20.0
5.0	60.0	7.5	1.5	100.0	20.0
5.0	180.0	7.5	1.5	100.0	20.0
5.0	300.0	7.5	1.5	100.0	20.0
5.0	420.0	7.5	1.5	100.0	20.0
5.0	540.0	7.5	1.5	100.0	20.0
8.0	60.0	7.5	1.5	100.0	20.0
8.0	180.0	7.5	1.5	100.0	20.0
8.0	300.0	7.5	1.5	100.0	20.0
8.0	420.0	7.5	1.5	100.0	20.0
8.0	540.0	7.5	1.5	100.0	20.0
5.0	300.0	5.5	1.5	100.0	20.0
5.0	300.0	11.0	1.5	100.0	20.0
5.0	300.0	7.5	3.0	100.0	20.0
5.0	300.0	7.5	4.5	100.0	20.0
5.0	300.0	7.5	1.5	0.0	20.0
5.0	300.0	7.5	1.5	50.0	20.0
5.0	300.0	7.5	1.5	100.0	10.0
5.0	300.0	7.5	1.5	100.0	40.0

overtopping pit with a cross-shore length of 2–4 km was set at the onshore side of the land.

The size of numerical cells was selected to ensure an appropriate balance between predictive accuracy and computational effort. Specifically, uniform cells of 2.00 m × 1.25 m × 0.50 m were applied to the vicinity of the surface of the land. The remainder of the entire domain was discretized using non-uniform cells with increasing width in the x and z directions. In the main solver, the surfaces of the bottom boundary, the side boundaries, the landward boundary, the quay wall, and the land were exposed to the slip condition. The Sommerfeld radiation condition was applied to the seaward boundary, and the constant-pressure condition was applied to the top boundary. In the VOF module, all boundaries were exposed to the gradient-free condition.

A single leading long-period wave with a generated tsunami height of H and a duration of T was adopted as an incident tsunami. Figure 2 shows an example of water surface fluctuation η at y = 0 m in front of the quay wall for H = 5.0 m, T = 300.0 s, h_l = 7.5 m, and h_f = 1.5 m with no buildings. In this study, the case of a generated tsunami height of H = 5.0 m, a duration of the tsunami of T = 300.0 s, a water depth at the LWL of h_l = 7.5 m, a freeboard of h_f = 1.5 m (equivalent to the still water depth of $h = h_l + 3.0 - h_f$ = 9.0 m), a distance to the buildings of x_b = 100 m, and a cross-shore length of the buildings of l_b = 20 m was selected as the reference case, and three different generated tsunami heights H (3.0, 5.0, and 8.0 m), five different durations of the tsunami T (60.0, 180.0, 300.0, 420.0, and 540.0 s), three different water depths at the LWL h_l (5.5, 7.5, and 11.0 m), three different freeboards h_f (1.5, 3.0, and 4.5 m), three different distances to the buildings x_b (0.0, 50.0, and 100.0 m), three different cross-shore lengths l_b (10.0, 20.0, and 40.0 m) were used in addition to the reference case (Table 1). Furthermore, as shown in Fig. 3, the shielding ratio R_s was changed to 0, 20, 50, 80, and 100% for each pattern, and the number of gaps between buildings n was changed to 1, 2, and 3 for R_s = 20–80%. In total, 253 cases were conducted. Here, the shielding ratio R_s represents the ratio of the long-shore width of the buildings with respect to the total width of the computational domain (100 m).

NUMERICAL RESULTS AND DISCUSSION

This study focused on the reduction rate of the inundation water volume R_v due to the existence of buildings with respect to the inundation water volume for no buildings under identical conditions of the generated tsunami height H, the duration of the tsunami T, the water depth at the LWL h_l, the freeboard h_f,

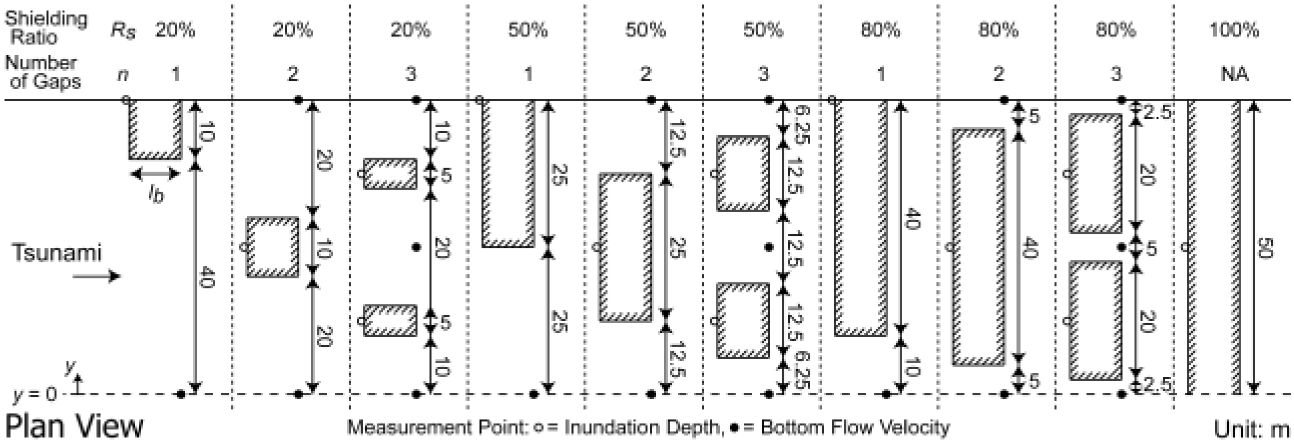

Fig. 3 Arrangement of the buildings with the shielding ratio of R_s = 20–100%

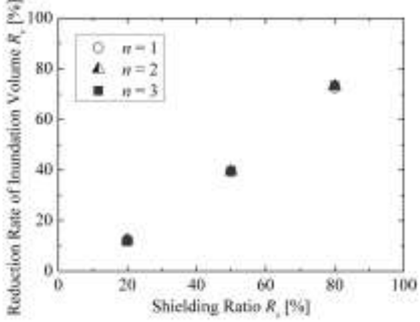

Fig. 4 Comparison of the reduction rate of the inundation water volume R_v in terms of the number of gaps between buildings n (H = 5.0 m, T = 300.0 s, h_l = 7.5 m, h_f = 1.5 m, x_b = 100 m, and l_b = 20 m)

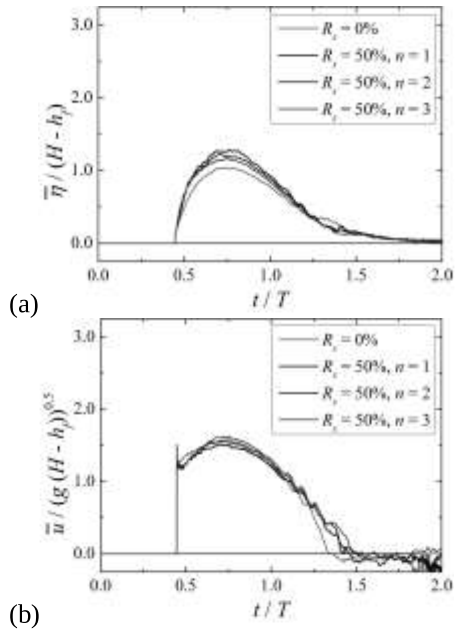

Fig. 5 Comparison in terms of the number of gaps between buildings n (H = 5.0 m, T = 300.0 s, h_l = 7.5 m, h_f = 1.5 m, x_b = 100 m, and l_b = 20 m): (a) cross-sectional averaged inundation depth $\bar{\eta}$; and (b) cross-sectional averaged cross-shore flow velocity $\bar{u}$

the distance to the buildings x_b, and the cross-shore length of the buildings l_b. Here, the inundation water volume represents the volume of water that inundates over the landward edge of the buildings ($x = x_b + l_b$).

Effects of Number of Gaps between Buildings

Figure 4 shows a comparison of the reduction rate of the inundation water volume R_v in terms of the number of gaps between the buildings n. As indicated in Fig. 4, there is little difference in the value of R_v under identical conditions of the shielding ratio R_s. Figure 5 shows the time series of the cross-sectional averaged inundation depth $\bar{\eta}$ and the cross-sectional averaged cross-shore flow velocity $\bar{u}$ at the seaward edge of the gap between the buildings ($x = x_b + l_b$ = 120 m). From Fig. 5(a), it is observed that the value of $\bar{\eta}$ / (H – h_f) decreases with an increase in that of n. Conversely, Fig. 5(b) indicates that the value of $\bar{u}$ / (g (H – h_f))$^{0.5}$ increases with that of n. Accordingly, as mentioned earlier, these two opposing effects result in the little effects of n on R_v.

Effects of Generated Tsunami Height

Figure 6 shows a comparison of the reduction rate of the inundation water volume R_v in terms of the generated tsunami height H. For $T \geq$ 300.0 s, Fig. 6(c)–(e) indicates that the value of R_v slightly decreases with an increase in H under identical conditions of the shielding ratio R_s. For T = 180.0 s, Fig. 6(b) shows that the trend of the change in R_v with an increase in H is not uniform. However, the difference in the value of R_v is smaller than that for $T \geq$ 300.0 s. Accordingly, the value of R_v is less affected by that of H. In contrast, for T = 60.0 s, Fig. 6(a) indicates that the value of R_v in the cases of H = 8.0 m is the largest among identical conditions of R_s. This is probably because the tsunami breaks offshore, and the broken

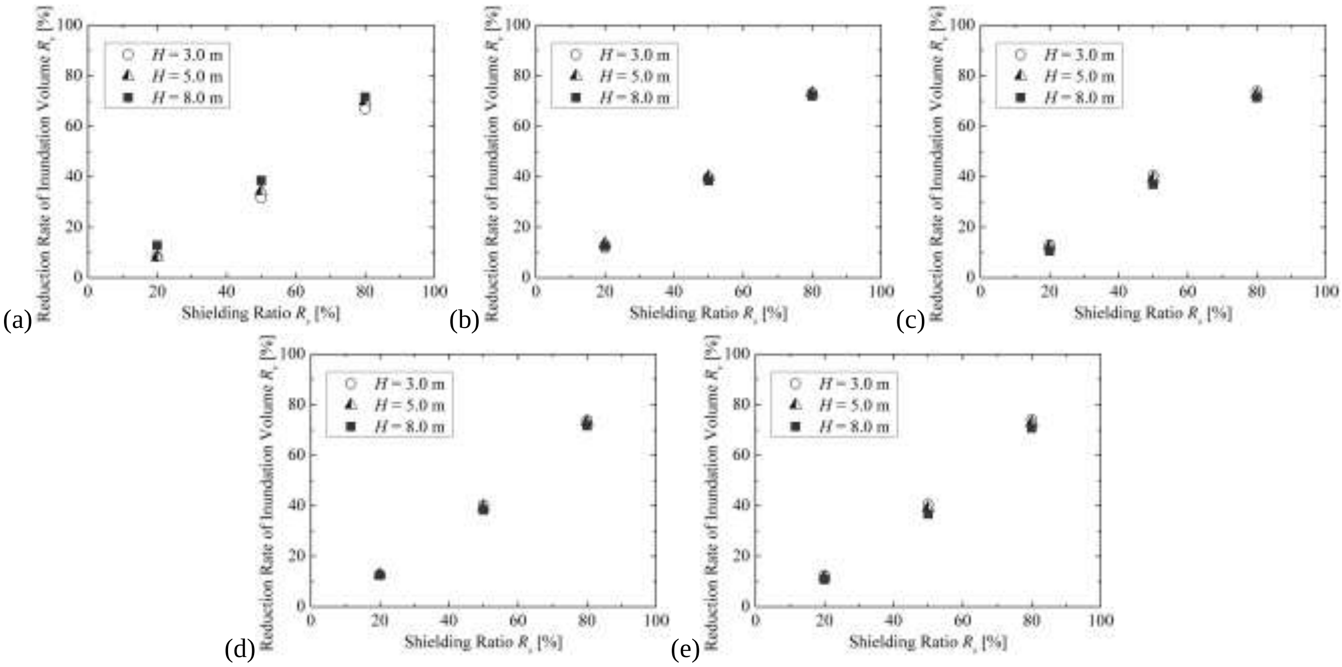

Fig. 6 Comparison of the reduction rate of the inundation water volume R_v in terms of the generated tsunami height H (h_l = 7.5 m, h_f = 1.5 m, x_b = 100 m, l_b = 20 m, and n = 1): (a) T = 60.0 s; (b) T = 180.0 s; (c) T = 300.0 s; (d) T = 420.0 s; and (e) T = 540.0 s

tsunami runs up onto the land for H = 8.0 m. Moreover, a comparison between the cases of H = 3.0 m and H = 5.0 m indicates that the value of R_v for H = 5.0 m tends to be slightly larger than that for H = 3.0 m. However, the duration of T = 60.0 s is relatively short, and accordingly the cases for T = 60.0 s is not appropriate for the modeling of tsunamis. As a result, from the results of Fig. 6(b)–(e), it is demonstrated that the shielding effects from the buildings can be reduced with an increase in H.

Effects of Duration of Tsunami

Figure 7 shows a comparison of the reduction rate of the inundation water volume R_v in terms of the duration of the tsunami T. For H = 3.0 and 5.0 m, it is observed from Fig. 7(a) and (b) that the value of R_v for T = 60.0 s is the smallest under identical conditions of the shielding ratio R_s. However, except for T = 60.0 s, there is little difference in the value of R_v, and accordingly the value of R_v is less affected by that of T. In contrast, as shown in Fig. 7(c), there is no significant change in the value of R_v for the cases of H = 8.0 m, including those of T = 60.0 s. From these results, it is revealed that the value of R_v remains practically constant with an increase in T except for the cases of T = 60.0 s.

Effects of Water Level at LWL

Figure 8 shows a comparison of the reduction rate of the inundation water volume R_v in terms of the water level at the LWL h_f. As shown in Fig. 8, there is little difference in the value of R_v due to the change in h_f. This result suggests that the water depth at the LWL h_f, i.e., the height of the quay wall, has little effect on R_v.

Effects of Freeboard

Figure 9 shows a comparison of the reduction rate of the inundation water volume R_v in terms of the freeboard h_f. From Fig. 9, it is observed that the value of R_v is less affected by that of h_f under identical conditions of the shielding ratio R_s. Since the change in h_f indicates that in the still water depth h under identical conditions of h_l, there are little effects of the tidal level on R_v.

Effects of Distance to Buildings

Figure 10 shows a comparison of the reduction rate of the inundation water volume R_v in terms of the distance to the buildings x_b. As shown in Fig. 10, the smaller the shielding ratio R_s is, the larger the reduction in R_v with an increase in x_b is. Accordingly, it is suggested that the shielding effects is higher for the buildings that are closer to the quay wall.

Effects of Cross-Shore Length of Buildings

Figure 11 shows a comparison of the reduction rate of the inundation water volume R_v in terms of the cross-shore length of the buildings l_b. It is observed in Fig. 11 that there is practically no change in the value of R_v with an increase in l_b under identical condition of the shielding ratio R_s. This result indicates that the value of R_v is less affected by that of l_b.

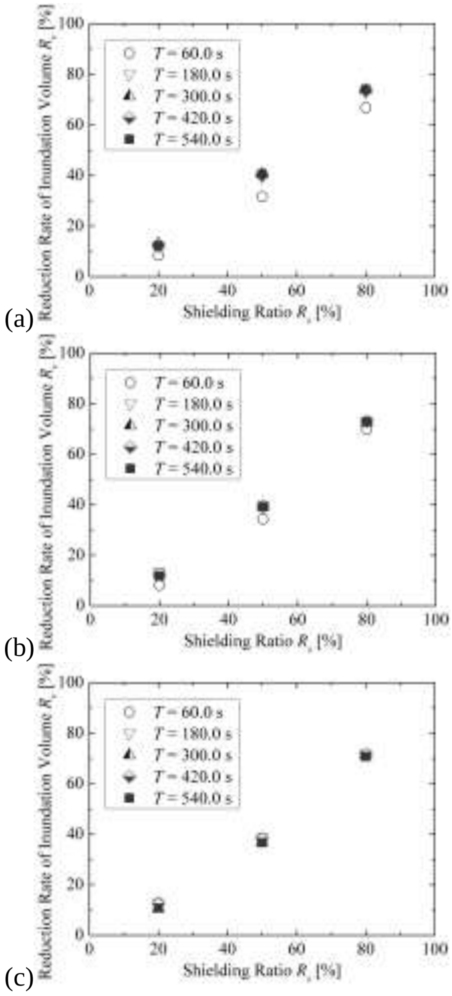

Fig. 7 Comparison of the reduction rate of the inundation water volume R_v in terms of the duration of the tsunami T (h_l = 7.5 m, h_f = 1.5 m, x_b = 100 m, l_b = 20 m, and n = 1): (a) H = 3.0 m; (b) H = 5.0 m; and (c) H = 8.0 m

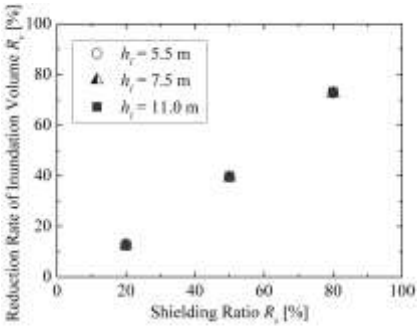

Fig. 8 Comparison of the reduction rate of the inundation water volume R_v in terms of the water depth at the LWL h_l (H = 5.0 m, T = 300.0 s, h_f = 1.5 m, x_b = 100 m, l_b = 20 m, and n = 1)

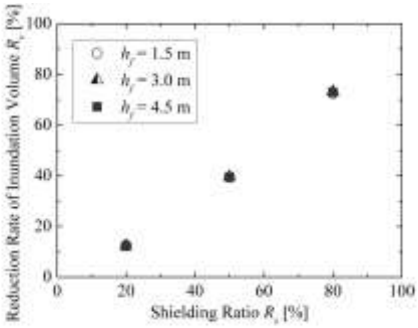

Fig. 9 Comparison of the reduction rate of the inundation water volume R_v in terms of the freeboard h_f (H = 5.0 m, T = 300.0 s, h_l = 7.5 m, x_b = 100 m, l_b = 20 m, and n = 1)

Approximation Equations for Estimating Reduction Rate of Inundation Water Volume

As mentioned earlier, the reduction rate of the inundation water volume R_v is practically independent on the number of gaps between the buildings n, the duration of the tsunami T (except when T = 60.0 s), the water depth at the LWL h_l, the freeboard h_f, and the cross-shore length of the buildings l_b. In contrast, the value of R_v is affected by that of the generated tsunami height H and the distance to the buildings x_b. Accordingly, Fig. 12 shows all cases with respect to H = 5.0 m and x_b = 100 m, along with the following approximation equation derived from the results of these cases:

For H = 5.0 m and x_b = 100 m,

$$R_v = 0.00427R_s^2 + 0.575R_s \quad \left(R^2 = 0.99971\right) \qquad (10)$$

Although it may not be possible to derive approximation equations at the same accuracy level as that of Eq. (10) because the number of cases is limited compared with that for H = 5.0 m, the approximation equations for H = 3.0 m and 8.0 m are derived in the same manner:

For H = 3.0 m and x_b = 100 m,

$$R_v = 0.00420R_s^2 + 0.586R_s \quad \left(R^2 = 0.99989\right) \qquad (11)$$

For H = 8.0 m and x_b = 100 m,

$$R_v = 0.00486R_s^2 + 0.510R_s \quad \left(R^2 = 0.99977\right) \qquad (12)$$

For H = 3.0, 5.0, and 8.0 m at x_b = 100 m, if the shielding ratio R_s is given, the value of R_v can be easily estimated from Eqs. (10)–(12) regardless of that of n, T h_l, h_f, and l_b. Consequently, it is quantitatively verified that impermeable rigid buildings located along the coasts act as multifaceted countermeasures by reducing the inundation water volumes due to tsunamis. This suggests that countermeasures against tsunamis can be evaluated in a comprehensive manner in terms of not only shore protection facilities but also such buildings.

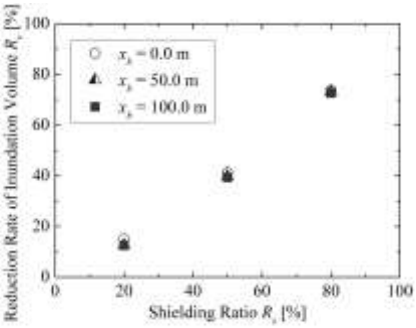

Fig. 10 Comparison of the reduction rate of the inundation water volume R_v in terms of the distance to the buildings x_b (H = 5.0 m, T = 300.0 s, h_l = 7.5 m, h_f = 1.5 m, l_b = 20 m, and n = 1)

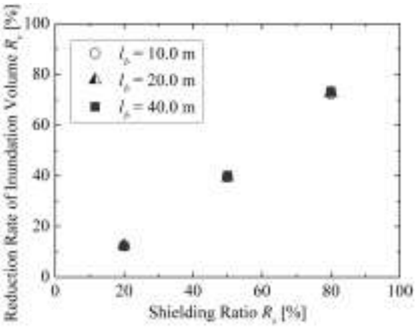

Fig. 11 Comparison of the reduction rate of the inundation water volume R_v in terms of the cross-shore length of the buildings l_b (H = 5.0 m, T = 300.0 s, h_l = 7.5 m, h_f = 1.5 m, x_b = 100 m, and n = 1)

However, the value of R_v tends to be reduced with an increase in x_b, as mentioned earlier. Furthermore, the value of R_v is presumed to decrease when the buildings have piloti-type structures and openings such as windows. Moreover, the number of cases is limited for H = 3.0 and 8.0 m, as explained in Eqs. (11) and (12). In addition, the computational conditions of n, h_l, h_f, x_b, and l_b are limited compared with those of H and T, as shown in Table 1. To evaluate the value of R_v for more conditions with sufficient accuracy, further numerical analyses need to be conducted in future studies.

Stability of Buildings

As revealed earlier, impermeable rigid buildings located along the coasts have the reduction effects of the inundation water volumes due to tsunamis. However, the buildings are simultaneously subject to wave force acting on their seaward surface and local scouring around their foundation. This section is devoted to investigating the stability of the buildings in terms of the inundation depth at their seaward side and the bottom flow velocity between the buildings.

Figure 13 shows the time series of the inundation depth η at the middle of the seaward side of the building, the position of which is represented using ° in Fig. 2. From Fig. 13, it is observed that the maximum value of η / (H – h_f) for the shielding ratio of R_s = 100% is approximately three times larger than that for no buildings (R_s = 0%).

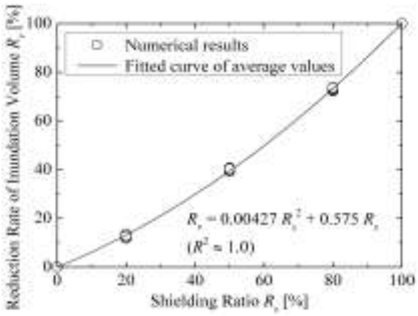

Fig. 12 Approximation equation for estimating the reduction rate of the inundation water volume R_v (H = 5.0 m, $T \geq$ 180.0 s, and x_b = 100 m)

This result is consistent with previous research such as Asakura et al. (2000). Furthermore, Fig. 13(a) indicates that the value of η / (H – h_f) is less affected by the number of gaps between the buildings n under identical conditions of R_s. In contrast, Fig. 13(b) shows that the value of η / (H – h_f) increases with that of R_s. Here, an increase in R_s also means an increase in the area subject to the wave force. These results infer that larger wave force can act on the seaward surface of the buildings for larger R_s.

Figure 14 shows the time series of the cross-shore bottom flow velocity u at the middle of the landward edge of the gap between the buildings, the position of which is represented using • in Fig. 2. From Fig. 14(a), it is observed that the value of $u / (g\,(H - h_f))^{0.5}$ rises with an increase in n under identical conditions of R_s since each gap is narrower for larger n. For the same reason, as shown in Fig. 14(b), the value of $u / (g\,(H - h_f))^{0.5}$ increases with that of R_s under identical conditions of n. From these results, it is inferred that larger-scale local scouring can be formed around the foundation of the buildings for larger R_s and n if the land is erodible.

As a result, it is essential to consider an appropriate balance between the reduction effects of the inundation water volume and the instability of the buildings caused by the wave force and the local scouring especially for larger R_s when designing the buildings along the coasts.

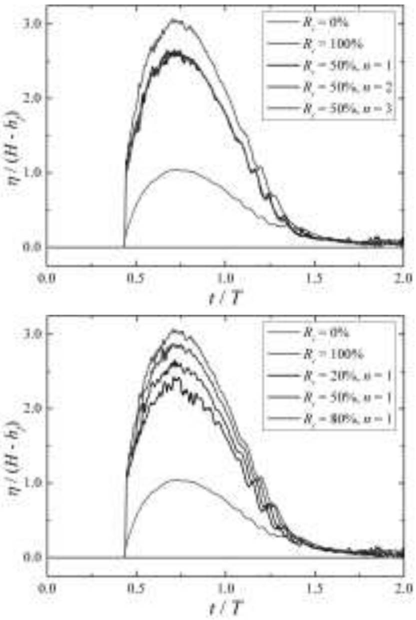

(a) (b)

Fig. 13 Comparison of the inundation depth η at the middle of the seaward side of the building (H = 5.0 m, T = 300.0 s, h_l = 7.5 m, h_f = 1.5 m, and x_b = 100 m): (a) the effects of n; and (b) the effects of R_s

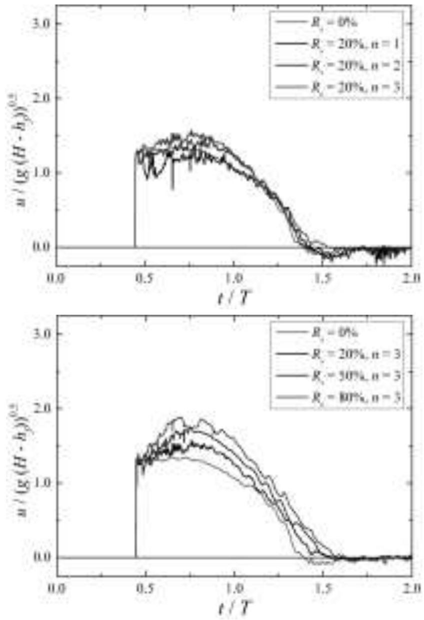

(a) (b)

Fig. 14 Comparison of the cross-shore bottom flow velocity u at the middle of the seaward edge of the gap between the buildings (H = 5.0 m, T = 300.0 s, h_l = 7.5 m, h_f = 1.5 m, and x_b = 100 m): (a) the effects of n; and (b) the effects of R_s

CONCLUDING REMARKS

A full-scale three-dimensional (3-D) numerical analysis was performed to quantitatively evaluate the effects of impermeable rigid buildings located near a vertical quay wall on the reduction of tsunami-induced inundation water volumes. For investigation, a run-up tsunami propagating through the buildings on a horizontal flat land behind the quay wall was analyzed in terms of the inundation water volume using a 3-D coupled fluid-structure-sediment interaction model. Numerical results showed that the inundation water volume can be reduced with an increase in a shielding ratio, i.e., the ratio of the long-shore width of the buildings with respect to the total width of the coastline, and accordingly the buildings located along the coasts have the reduction effects of the inundation water volume. This suggested that countermeasures against tsunamis can be evaluated in a comprehensive manner in terms of not only shore protection facilities but also such buildings. Based on the numerical results, approximation equations were proposed to predict the reduction rate of the inundation water volume from the shielding ratio and the tsunami height. However, numerical results also showed that the inundation depth at the seaward side of the buildings and the cross-shore bottom flow velocity at the gaps between the buildings increase with the shielding ratio, suggesting an increase in wave force acting on the buildings and the onset of local scouring around their foundation when the shielding ratio is large.

Consequently, it is essential to consider an appropriate balance between the reduction effects of the inundation water volume and the instability of the buildings caused by the wave force and the local scouring when designing the buildings along the coasts.

REFERENCES

Asakura, R., Iwase, K., Ikeya, T., Takao, M., Kaneto, T., Fujii, N., and Omori, M. (2000). An experimental study on wave force acting on on-shore structures due to overflowing tsunamis. Proc., Coastal Eng., JSCE, 47: 911-915 (in Japanese).

Brackbill, J. U., Kothe, B. D., and Zemach, C. (1992). A continuum method for modeling surface tension. J. Comp. Phys., 100: 335-354.

Coastal Development Institute of Technology (CDIT) (2001). Research and Development of Numerical Wave Flume (Super Roller Flume for Computer Aided Design of Maritime Structure), CDIT, 296 p. (in Japanese).

Horiuti, K. (1997). A new dynamic two-parameter mixed model for large-eddy simulation. Phys. Fluids, 9(11): 3443-3464.

Kajishima, T. and Takiguchi, S. (2002). Interaction between particle clusters and particle-induced turbulence. Int. J. Heat and Fluid Flow, 23: 639-646.

Kawasaki, K. (1999). Numerical simulation of breaking and post-breaking wave deformation process around a submerged breakwater. Coastal Eng. J., JSCE, 41(3-4): 201-223.

Kunugi, T. (2000). MARS for multiphase calculation. Comp. Fluid Dynamics J., 9(1): 1-10.

Mizutani, N., McDougal, W. G., and Mostafa, A. M. (1996). BEM-FEM combined analysis of nonlinear interaction between wave and submerged breakwater. Proc., 25th Int. Conf. on Coastal Eng., ASCE, 2377-2390.

Nakamura, T., Yim, S. C., and Mizutani, N. (2011). Numerical simulation on local scouring around bottom-mounted movable short cylinder. Proc., Coastal Structures 2011, ASCE, C4-087, 12 p.